Plasma Sources Sci. Technol. **16** (2007) 635–642 doi:10.1088/0963-0252/16/3/024

Fabry–Pérot lineshape analysis in an optically thick expanding plasma

E Pawelec[1,3], V Caubet-Hilloutou[2] and S Mazouffre[2]

[1] Opole University, Oleska 48, Opole, Poland.
[2] ICARE-CNRS, 1C Avenue de la Recherche Scientifique, 45071 Orléans, France

E-mail: ewap@uni.opole.pl

Received 29 January 2007, in final form 13 May 2007
Published 3 August 2007
Online at stacks.iop.org/PSST/16/635

Abstract
In this work the authors present Fabry–Pérot measurements of Ar atom spectral line profiles originating from the expansion of an Ar–N_2 thermal plasma into a low pressure environment. The plasma is characterized by strong density, temperature and velocity gradients and it offers a high degree of light absorption for some gas mixtures. First, it is demonstrated that the Abel inversion method cannot be applied under such conditions even if absorption is absent. Second, two approaches are examined to obtain plasma parameters in the case of an optically thick expanding plasma. It is shown that velocity and temperature development along the jet radius can be inferred from experimental lineshapes when radiation production and absorption are taken into account in the core and in the surroundings of the jet.

1. Introduction

Optical spectroscopy, either passive or active, is a favorite tool for studying plasma sources as it only weakly, if at all, disturbs the plasma medium. Moreover, it can be used for the determination of various plasma parameters and the properties. The most extensively measured variables are the intensity and the profile of emitted or absorbed spectral lines, from which it is possible to assess the density, the temperature and the velocity of the observed particles. Most common methods of plasma tomography are based on the assumptions of low density and low plasma velocities, at least in the direction of the line of sight. In many cases such assumptions are valid. Unfortunately, there are also many plasma sources for which the most common assumptions are not true. Even a strongly rarefied plasma source can exhibit significant absorption for certain wavelengths, especially if the plasma source is relatively large. There are also many sources of plasma where the atom or the molecule velocity in the direction of the observation is definitely non-zero. This is as true for many astrophysical sources as for laboratory ones, which are in most cases expanding, e.g. plasma jets and beams, laser-produced plasmas, solar flares, exploding-wires, to name only a few [1–3].

[3] Author to whom any correspondence should be addressed.

The case of an optically thick plasma has been studied long in certain types of experiments [4]. Yet, the analysis is often performed under conditions such that either gradients of density and temperature in the direction of observation can be neglected or an assumption about the plasma state can be made, such as local thermodynamic equilibrium. One of the most recent and most comprehensive approaches to treat light absorption in an optically dense expanding plasma medium is described in [5]. Though a few works are reported in the literature, see [6–8], the influence of the velocity on data extraction from optical measurements is usually not taken into account, especially if the velocity is not uniform. The difficulty in accounting for the departure from the ideal case, i.e. an optically thin plasma with cylindrical symmetry at rest, originates from the fact that the Abel inversion method cannot be directly applied [9–11]. Studies dealing with the generalization of the method, e.g. to cope with the breaking of the cylindrical symmetry, are available [12–14]; however, to include light absorption and particle velocity is not straightforward from a mathematical point of view.

In this paper we analyze the signals for both optically thick and optically thin expanding plasmas, testing the limits of the applicability of the Abel inversion method. We then suggest an approach that allows us to obtain a proper estimation of plasma parameters in the case of an optically thick expanding plasma. This approach is based on the modeling of radiation transport

in the medium and on comparing numerical results with the measurement outcomes. The analysis also points out the pitfall of common assumptions as the uninverted—line of sight integrated—optical measurements solely give the 'averaged' values of plasma parameters. It is clearly demonstrated that standard data analysis methods can lead to strong over- or underestimation of real local values [15, 16].

2. Plasma source and plasma expansion

The plasma source used in this work is a water-cooled vortex stabilized dc-arc torch [17]. The torch is equipped with a tungsten cathode and with a convergent (30°)–divergent (25°) copper nozzle that acts as a grounded anode. The length of the divergent part is 5 cm and the exit diameter of the nozzle is 4.8 cm. The arc extends from the tip of the cathode through a 4 mm diameter molybden throat and attaches diffusely to the nozzle. The arcjet can be operated in a wide range of currents (10–300 A) and gas flows (5–50 slm). The plasma torch can be run for several hours, the lifetime being determined by the cathode erosion. Gases are fed through mass flow controllers directly into the cathode area. The torch is mounted on an arm that can be moved in the vertical and the horizontal directions. Thermal plasma is created in an Ar–N_2 gas mixture. Subsequently the plasma expands from the arcjet into a low pressure stainless steel vessel, which is 4.3 m long and has a diameter of 1.1 m. Standard operating conditions for this experiment are a 100 A direct current, a cathode–anode voltage of 45 V, an Ar gas flow of 20 slm (0.6 g s^{-1}) and a N_2 gas flow of 5 slm (0.1 g s^{-1}). The pressure in the cathode area is 76 kPa and the background pressure in the vessel is 2.5 Pa. The overall plasma source efficiency is around 60%.

As the plasma expands through a nozzle from a high pressure region into a low pressure region, a well-defined free jet shock wave structure is formed [18]. The plasma first flows supersonically: the Mach number reaches 1 at the nozzle throat and the flow is supersonic in the divergent portion. In this flow domain, the temperature drops and the drift velocity increases due to energy conservation. In the same region, the particle density along a streamline decreases because of the increase in the jet diameter. In the case of an underexpanded jet, the flow domain is limited by a barrel shock wave behind the nozzle exit. At some distance from the source, depending among others upon the background pressure, the side shock waves interact with one another on the jet axis. Depending upon both the Mach and the Knudsen number values, two types of shock wave patterns are possible [19]. A Mach disc associated with an oblique reflected shock can be created, through which the flow undergoes a supersonic to subsonic transition: Mach reflection [20]. Under specific conditions, i.e. a large Mach number and high level of rarefaction, the Mach disc vanishes and the flow experiences a supersonic to supersonic transition with a slight decrease in the Mach number magnitude: regular reflection [21]. The latter process can occur several times over appreciable distances leading to the appearance of several stationary expansion cells. Beyond the overall shock region, the plasma flows subsonically at constant static pressure. Under our flow conditions, the shock wave structure results from regular reflexion [21].

3. Experimental arrangement

A Fabry–Pérot (FP) interferometer may be regarded as a very narrow bandwidth optical filter. It is often used to examine the detailed structure of spectral lines. A detailed description of the experimental arrangement can be found in [22, 23]. After being collected by a lens, light emanating from the plasma jet is directed towards the optical bench by means of a multimode optical fiber. A similar fiber is also used to carry a part of the light emitted by a 100 Hz low pressure argon lamp. The two optical fibers are combined by means of a three port 50/50 fiber coupler. The light leaving the fiber is collected by a lens in such a way that a collimated beam of light is formed. The parallel beam passes a plane FP cavity limited by two 2.5 cm diameter apertures. Behind the cavity, the transmitted light is focused onto a pinhole in order to select solely the central interference ring. The diaphragm is imaged onto the entrance slit of a 40 cm monochromator that acts as a rough wavelength selector to separate the line to be studied from the rest of the plasma spectrum. A photomultiplier tube is used as a light detector. The delivered signal is registered with an oscilloscope connected to a computer. The FP cavity (RC110 from Burleigh) is a piezo-scanned type: the length as well as the alignment of the cavity is controlled by applying high voltage onto piezoelectric mirror mounts. An accurate frequency scan is realized by smoothly varying the mirror position with a high voltage ramp. All measurements presented in this paper have been obtained with a cavity scanning frequency of 10 Hz. Each spectrum results from averaging over 500 cycles.

The distance between the two dielectric mirrors of the FP cavity is 15.1 mm, i.e. the free spectral range of the cavity is equal to 9.924 GHz. In the spectral range of interest, the mirror reflectivity is around 99%. The mirrors are flattened to $\lambda/200$. Therefore, the net finesse of the FP cavity is around 180. The instrumental finesse that characterizes the resolving power of the complete FP bench, accounting for losses induced by pinholes and lenses, is found to be around 65 [22]. In other words, the FP setup allows achieving a spectral resolution of about 0.15 GHz (0.4 pm). A lens with a 100 mm focal length images the jet onto the entrance of a multimode optical fiber connected to the FP bench. The magnification is 0.125 which corresponds to a spatial resolution of 3 mm in the radial direction. The line of sight is oriented at 90° with respect to the jet symmetry axis, see figure 1. Such a configuration enables us to measure the perpendicular velocity and the temperature in a plasma column exhibiting cylindrical symmetry. However, FP spectroscopy does not allow us to carry out measurements with a good spatial resolution. The field depth of our observation branch is about 25 cm, i.e. the field depth is larger than the plasma jet diameter. As a consequence, the observed line profile is a result of an integration along the line of sight.

Two Ar line profiles are analyzed with the FP setup. The Ar I line at 763.51 nm corresponds to the $2p_6 \rightarrow 1s_5$ transition. The Ar I line at 738.40 nm corresponds to the $2p_3 \rightarrow 1s_4$ transition. Note that the $1s_5$ state is metastable, whereas the $1s_4$ state is resonant. These two Ar lines were chosen as they are well isolated, they are both relatively strong transitions and the PMT quantum efficiency is relatively high below 800 nm. The temperature is deduced from the Doppler broadening of the line taking into account the apparatus width.

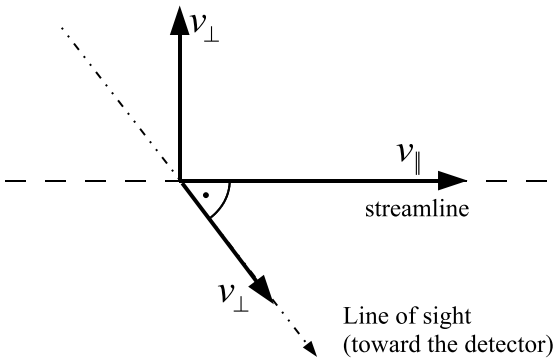

Figure 1. Observation configuration for FP interferometry. The line of sight is directed at 90° with respect to the jet axis. $v_\perp$ denotes perpendicular (radial) velocity; $v_\parallel$ denotes axial velocity parallel to the jet streamline.

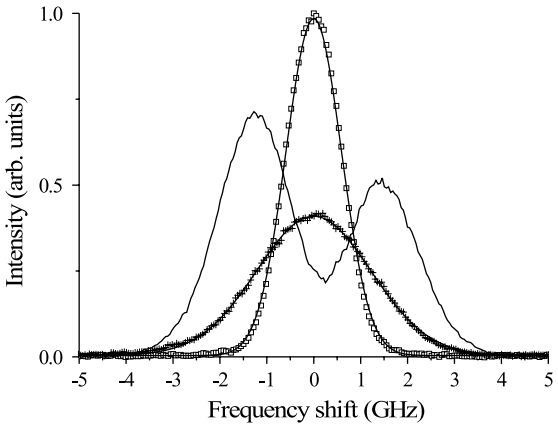

Figure 2. Profiles of the Ar 763 nm line measured with the FP bench: low pressure argon lamp (squares) and plasma at the arcjet nozzle outlet. In low-absorption conditions, the Ar line profile is Gaussian (crosses). When the seeded N_2 fraction is small (solid line) the 763 nm radiation is strongly absorbed around the line centre ($\phi_{Ar}/\phi_{N_2} = 6$ in this example).

As can be seen in figure 2, when the seeded N_2 fraction is small, the radiation is strongly absorbed around the spectral line centre due to the production of a large amount of excited Ar atoms [21]. This phenomenon is especially visible in the case of the 763 nm Ar line which is linked to the longlived Ar[$1s_5$] state. The N_2 molecules seeded fraction serves to vary the argon atom excited state content in the jet by way of an efficient charge-exchange reaction [21]. Hence changing the amount of N_2 molecules permits us to monitor the degree of light absorption.

4. Data treatment with the Abel transform method

In the case of optically thin plasmas with radial symmetry, the most frequent method for determining local plasma parameters by emission spectroscopy is the so-called Abel inversion method. To derive the local emission coefficient ϵ from the intensity I' of the light integrated over the line of sight, one has to calculate the Abel integral [24]:

$$\epsilon(r) = -\frac{1}{\pi}\int_r^R \frac{I'(y)\,\mathrm{d}y}{\sqrt{y^2 - r^2}}, \qquad (1)$$

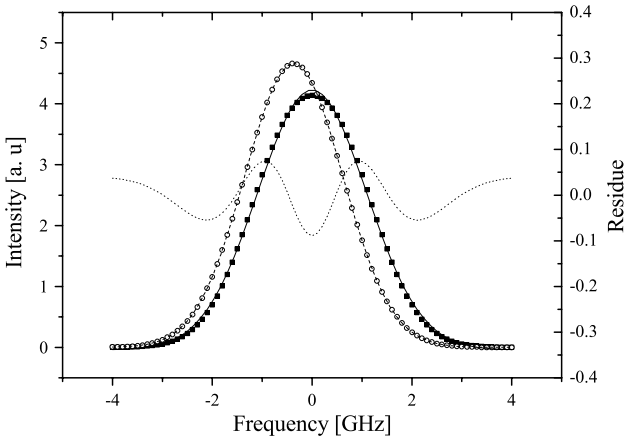

Figure 3. Theoretical profiles of the emission coefficient ϵ at a given location r obtained with equation (2) (circle) and with the Abel inversion method (square) for an optically thin flowing plasma with large radial velocities. Solid lines are Gaussian fits. The Abel inverted profile departs from a Gaussian function as shown by the residue (dotted line).

where R is the source radius, r a radial coordinate and y a Cartesian coordinate perpendicular to the line of sight. The aforementioned integration can be performed either for each wavelength separately to retrieve the line profile (point-by-point Abel inversion) or for the total line intensity. These two methods are used in plasma diagnostics. Abel inversion based on total line intensity is much easier; however, the line profile contains more information, so the point-by point method is also widely used.

In the case of expanding radially-symmetric plasma jet, the situation complicates as spectral lines that originate from different positions are shifted in frequency due to the Doppler effect. Even if the value of the velocity vector depends only on the radial coordinate, the frequency shift $\Delta\nu$ depends also on the angle between the velocity vector and the observation axis as $\Delta\nu = \vec{k}\cdot\vec{v}$ where $\vec{k}$ is the line of sight alignment vector. The observed shift is therefore not symmetric about the jet axis. As a consequence, the profile of the emission coefficient ϵ must be described as

$$\epsilon(\nu, r, \varphi) \propto \frac{1}{\Delta\nu_D(r)} \exp\left(-4\ln 2\left(\frac{\nu - \nu_0 - \delta\nu_D(r,\varphi)}{\Delta\nu_D(r)}\right)^2\right), \qquad (2)$$

where $\Delta\nu_D$ is the Doppler width of the profile, ν_0 is the non-shifted line centre frequency, $\delta\nu_D$ is the Doppler shift and φ is the angular coordinate. Only the radial velocity component is relevant in the calculation as the source is observed aside: the axial velocity gives only a negligible perpendicular Doppler effect. This equation shows that the emission coefficient does depend upon φ in contradiction with the assumptions allowing us to perform the Abel inversion. It proves that in the case of non-negligible plasma flow the line profiles obtained by performing 'classical' Abel inversion are incorrect—as shown in figure 3. This figure displays two theoretical profiles of the emission coefficient ϵ at a given location r obtained with equation (2) and with the Abel inversion method for an optically thin flowing plasma with large radial velocity components. The temperature and radial velocity curves were

arbitrarily chosen. The constraints for the velocity profile are the radial velocity component is zero at $r = 0$ and the plasma expansion exhibits radial symmetry. Results shown in figure 3 indicate that the temperature obtained from the width of computed lines is not correct when the Abel inversion is applied. Naturally the velocity is not found again when using equation (1). Nevertheless, the Abel inversion is valid to calculate the total line intensity, i.e. integrated over frequency, as the Doppler shift does not play any role in that case. This allows us to determine the density of excited atomic levels, which can be used to assess the temperature by means of a Boltzmann plot or for plasma diagnostics by applying a collisional–radiative model.

Abel inversion is therefore not applicable for determining lineshapes in expanding plasmas. As a consequence it cannot be employed for extracting Doppler broadening. Yet it remains a powerful tool to determine excited state density. As we will see, the situation is much worse when the plasma is optically thick. In that case, the relation between the line intensity and the emission coefficient is no more given by equation (1) and one must turn towards a more complex approach.

5. Simplified model of radiation transport throughout the jet

In the experiment described here, spectral lines emitted by the plasma near the nozzle exit were strongly reabsorbed for most of the utilized gas mixtures, see figure 4. They were also not symmetric in frequency—the blue part of the measured profile was always weaker. The observed profiles did not depend on the line of sight orientation. As the plasma jet is placed horizontally, it can be viewed either in the horizontal direction perpendicular to the jet axis or in the vertical direction.

Following the approach originally developed by Meulenbroeks [5], a simple model was set up in order to explain the origin of asymmetric FP lineshapes. The plasma jet cross-section is seen as consisting of two parts: a hot emitting core surrounded by a colder absorbing gas, as shown in figure 5. These two plasma volumes can be characterized by two Gaussian distributions, a wide profile for the emitting core and a narrow one for the absorbing layer. Somewhat more complicated is the explanation for the skewness of the lineshapes, which is connected with the radial velocity profile [21]. In the centre of the jet the radial velocity is very small and it increases with the distance from the axis. The emitting core has the maximum emissivity at $r = 0$ and is axially symmetric, so the emitting line will be centred at the frequency of the atom at rest. The colder gas around it moves outwards. In the case when the line of sight crosses the jet centre, movement of the cold fringe is directed towards the observer with an average velocity of the order of some hundreds of $\mathrm{m\,s^{-1}}$ [21]. Due to the expansion phenomenon, the gas between the emitting core and the observer always moves towards the observer, see figure 5.

In order to simplify the treatment, we assume that both the core and the absorbing fringe are uniform with constant density, velocity and temperature. Within the core of the jet the velocity is zero. The temperature is uniform; however, it differs inside and outside the core. The skewness of the profiles can therefore be explained by the difference in the central frequency of the Gaussian profiles describing the emission of

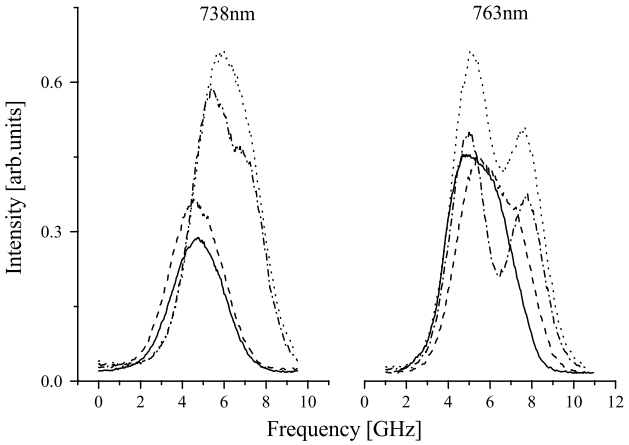

Figure 4. Examples of measured lineshape of two argon lines under various plasma conditions: 738 nm and 763 nm lines observed at $z = y = 0$: solid line—20 Ar/5 N_2, dashed line—20 Ar/4 N_2, dotted line—25 Ar/3 N_2, dashed–dotted line—29.2 Ar/2.2 N_2. Gas flow rates are in units of slm.

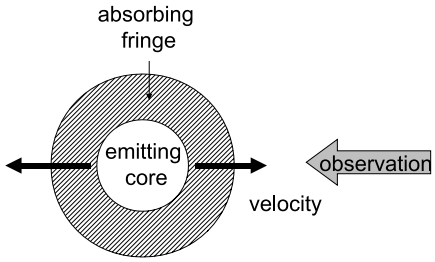

Figure 5. A schematic view of the simple model used to explain the asymmetric line profiles. The plasma cross-section is envisaged as consisting of two distinct parts.

the hot core and of the cold surroundings. The difference is due to the Doppler shift of the profile describing absorption in the moving fringe. The model gives the following function for the resulting line profile:

$$I(\nu) \propto N_{\mathrm{emit}}\, l_{\mathrm{emit}}\, e^{\left[-\left(\frac{\nu-\nu_0}{w(T_{\mathrm{emit}})}\right)^2\right]} \times e^{-\alpha\, N_{\mathrm{abs}}\, l_{\mathrm{abs}}\, \exp\left[-\left(\frac{\nu-\nu_0+\Delta\nu_{\mathrm{dopp}}}{w(T_{\mathrm{abs}})}\right)^2\right]}, \tag{3}$$

where the subscripts emit and abs refer to the emitters and the absorbers, respectively. In equation (3), N is the density, l is a length, T is the temperature, w is the width of the line profile, α is the absorption coefficient and $\Delta\nu_{\mathrm{dopp}}$ is the Doppler shift of the absorbing curve due to the plasma radial expansion. The shape of a line profile depends upon many processes such as the Doppler effect, the pressure broadening due to neutrals and the Stark broadening due to electrons. Under our conditions, the Doppler broadening dominates; hence the width of the profile is proportional to the square root of the translational temperature.

In figure 6, a double-Gaussian curve described by equation (3) is fitted to several experimental profiles measured for different positions of the observation axis. In this figure, $y = 0$ corresponds to a measurement with the observation axis oriented along the jet diameter. Settings of the FP bench are the same for all spectra. The light intensity decreases when moving away from the horizontal plane. Data derived from

the fit to a double-Gaussian function are given in table 1. As can be seen in figure 6, the simplified model based on two distinct plasma regions enables us to reproduce the observed line profiles. However, as shown in table 1, the parameters, especially for the absorbers, start to be very uncertain for large values of the y coordinate. As a consequence, values obtained with this approach for T and v in the two considered regions of the plasma jet are not very accurate, as discussed in the last section of this paper.

6. A more realistic model of radiation transport

Splitting the plasma jet into two regions through which emitters and absorbers properties are constant prevent assessing the radial development of plasma parameters from the FP lineshapes. One therefore needs a more subtle model (similar in idea to the ones described in [25, 26]) of the plasma jet that accounts for density, temperature and velocity gradients: instead of solely considering two distinct regions the plasma must be decomposed into a large number of elementary cells. Hence, the plasma is described as a 2D rectangular mesh of 40 × 40 nods assuming cylindrical symmetry. Cartesian coordinates are chosen to facilitate numerical integration along the observation axis. Computed line profiles contain 80 points within a frequency range of a few gigahertz around the unperturbed frequency (null frequency shift). Plasma parameters depend on the radial coordinate defined as $r = \sqrt{x^2 + y^2}$. Evolution with r of the argon atom temperature and velocity has been measured by way of laser spectroscopy under identical conditions [21]. In contrast, the density of argon atoms in different atomic levels is unknown. In order to complete the model the shape of density profiles is estimated after several works on gas and plasma expansions, see, e.g. [27,28]. Finally, $T(r)$ and $n(r)$ are Gaussian, whereas $v_r(r)$ exhibits a more dispersive shape. The three spatial distributions are characterized by their own set of parameters, e.g. maximum value and width. The simulated lineshapes are obtained using the discretized version of the following equation:

$$I(\nu, y) \propto \int_{-R}^{R} \epsilon(\nu, x, y) \times \exp\left(-\int_{x}^{R} \alpha(\nu, x', y)\, \mathrm{d}x'\right) \mathrm{d}x, \tag{4}$$

where ϵ is the local emission coefficient of the plasma and α is the local absorption coefficient. R is the jet radius. The equation describes the fact that the amount of light collected by the detector located at the distance y from the jet axis is the sum of all the light produced along the line of sight. However, on its way to the detector the light is absorbed at each point up to the jet boundary, see figure 7. In order to compare numerical outcomes with measurements, the model must take into account the spectral response and the resolution of the optical system. The easiest way is to consider an ideal FP interferometer with an Airy function as an apparatus function. The problem in obtaining information about plasma parameters with this approach is that some of the parameters introduced in the model have a similar impact upon the computed lineshape. As can be seen in figure 8, increasing the maximum plasma velocity gives the same result as changing the plasma temperature as one obtains nearly identical FP lineshapes with very different pairs of parameters. Note that for this calculation $v(r)$ is the one given in figure 10 and $T(r)$ is constant. The difference between the profiles is of the order of 2%, see figure 8. Such a small spread can easily be hide due to noise or to the fact that the apparatus function can slightly change during the measurements, hence a large uncertainty on $T(r)$ and $v(r)$. Curves shown in figure 8 are very similar; fortunately such a similarity solely exists if light is not absorbed at all. Strongly absorbed lines are more interesting for the validation of the plasma model as they contain more information. Weak absorption means no information about the colder, less luminous regions of the jet. Moreover, there is one feature of the profile that does not depend on the plasma temperature, but only on the velocity: the difference in the centre frequency of the absorption and emission curves. This feature can therefore help in determining the atom velocity and the temperature.

To check the validity of the model based on equation (4), measured and computed Ar lineshapes are compared in

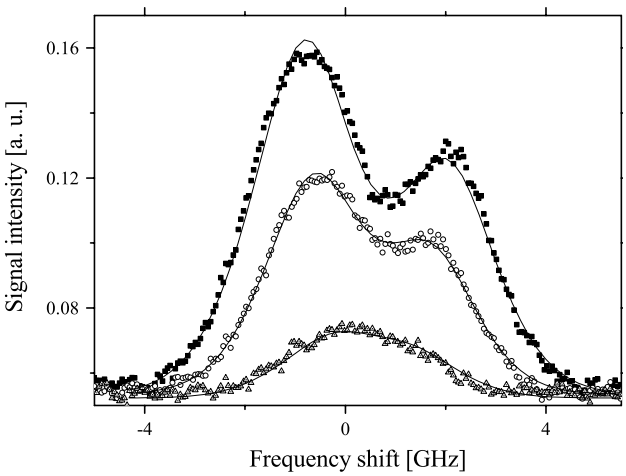

Figure 6. Profiles of the 763.5 nm Ar line measured with the FP bench at the nozzle outlet for various vertical positions: $y = 0$ cm (square), $y = 1$ cm (circle) and $y = 2$ cm (triangle). Plasma conditions are: 29.2 slm of Ar, 2.2 slm of N_2 and a 100 A current. The solid lines correspond to best fits to experimental data using a simple two-region model for the plasma jet.

Table 1. Data derived from fits to a double-Gaussian function; two-region model, see figure 6. The area A of the Gaussian curves is proportional to $N \times l$. Error bars originate from the fitting procedure.

y (cm)	$FWHM_{emit}$ (GHz)	A_{emit} (a.u.)	$FWHM_{abs}$ (GHz)	A_{abs} (a.u.)	$\Delta\nu_{dopp}$ (GHz)
0	3.63 ± 0.06	15.76 ± 0.79	2.14 ± 0.06	150.9 ± 9.2	0.37 ± 0.02
1	3.19 ± 0.05	10.18 ± 0.6	1.89 ± 0.07	125 ± 11	0.32 ± 0.02
2	3.02 ± 0.08	2.43 ± 0.21	1.51 ± 0.30	47 ± 21	0.27 ± 0.08

figure 9. A full frequency shift versus the y position map (function defined by equation (4)) is shown in figure 9 for the Ar transition at 763.5 nm as well as cross-sections. Parameters used for calculations are shown in figure 10. Note that experimental data are identical in figure 6 and in figure 9. With the two-region model, parameters can vary from one fit to another; moreover T is different for emitters and absorbers. In contrast, with the more elaborated model based on equation (4), all curves result from one single set of parameters with the temperature and the velocity of both emitters and absorbers given by the same $T(r)$ and $v(r)$ curves. As can be seen in figure 9, the agreement between experimental and computed curves is rather good. Distributions of $T(r)$, $v(r)$ and $n(r)$ are obtained from a fit of computed $I(\nu, y)$ profiles to a data set; as a consequence the uncertainty is still high. It is estimated to be of the order of 25% for the temperature and the velocity. Note that in figure 10 the density values are not necessarily in scale: no absolute measurements of the light intensity were carried out and the integration lengths are unknown.

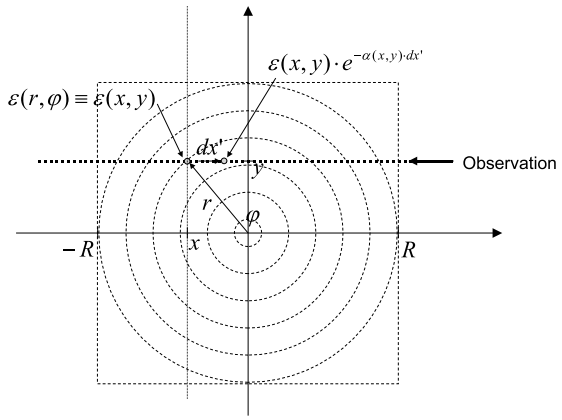

Figure 7. Integration of the light intensity in an absorbing and emitting cylindrical plasma source.

7. Results and discussion

The first point to be discussed is the assumption on which the two models rely. The two-region model distinguishes between two, spatially distinct, plasma regions with a sharp boundary: one through which radiation is generated and one through which light absorption occurs. Moreover, line profiles of emission/absorption do not depend on the spatial position, i.e. the Doppler width and the Doppler shift are constant within the concerned region. If the model is valid, the results should be the following. The area of the emitting Gaussian which is proportional to $N_{\text{emit}} \cdot l_{\text{emit}}$ should decrease with y as the integration path length decreases. The area of the absorbing Gaussian should slightly increase as l_{abs} increases for off-axis measurements. The widths of both profiles should stay unchanged. Results presented in section 5 are not in accordance with expectations. The area of the emitting and the absorbing Gaussian curves decreases. Therefore, we cannot assume that nearly all absorbers are located around the emitting core. In a similar manner, the width of the two Gaussian curves decreases meaning that the temperature does vary within the two regions. The question of a sharp boundary between the two regions must also be addressed. In this work, the shift in the centre frequency of emitting and absorbing profiles originates in the radial velocity, not in the electron density as in [5]. Emitters are at rest, whereas absorbers move in the radial direction towards the observer. As revealed by laser induced fluorescence measurements [20,21], Ar atom radial velocity varies smoothly from the jet axis up to the jet boundary where it reaches zero. There is no reason why the radial velocity component should change suddenly and drastically and should solely affect absorbers. Moreover, as

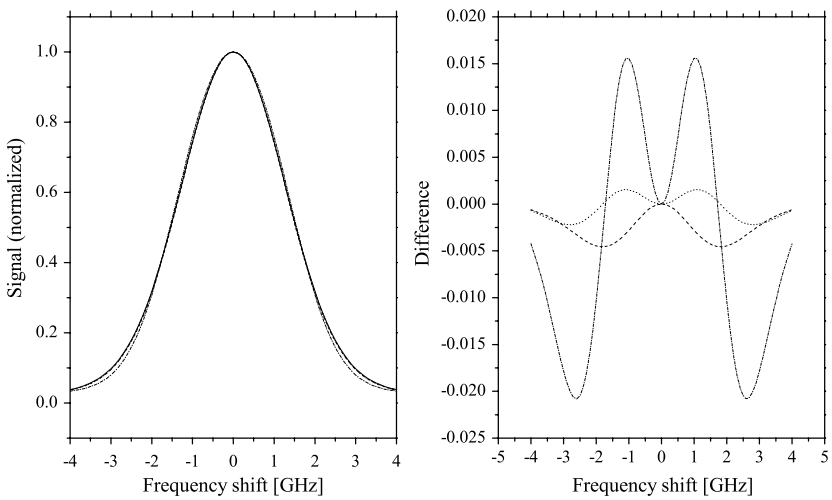

Figure 8. FP lineshapes simulated with two different T and $\delta\nu$ pairs (only the maximum value is considered here). Solid line: $T = 4500$ K and $\delta\nu = 0$ GHz, dashed line: $T = 4200$ K and $\delta\nu = 0.5$ GHz, dotted line: $T = 3500$ K and $\delta\nu = 1$ GHz, dashed–dotted line: $T = 1900$ K and $\delta\nu = 1.5$ GHz. All profiles are almost perfectly superimposed. The difference between the profile with no Doppler shift and the rest is given in the right figure.

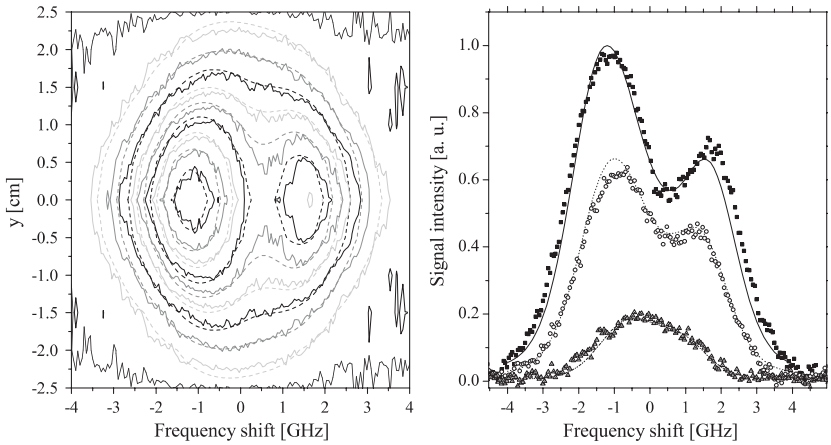

Figure 9. Experimental and computed profiles of the 763.5 nm Ar line at the nozzle outlet. Plasma conditions are 29.2 slm of Ar, 2.2 slm of N_2 and a 100 A current. Left: full $I(\Delta\nu, y)$ map. Numerical outcomes are given by dashed lines. Right: cross-sections at various vertical positions: $y = 0$ cm (square), $y = 1$ cm (circle) and $y = 2$ cm (triangle). Numerical outcomes correspond to solid lines.

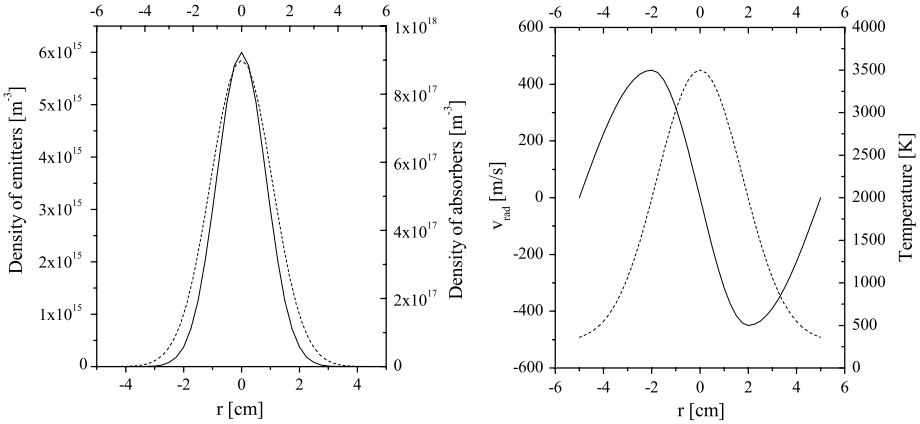

Figure 10. Distribution of plasma parameters used in calculations outcomes of which are shown in figure 9. Solid, respectively, dashed lines correspond to left, respectively, right vertical axis.

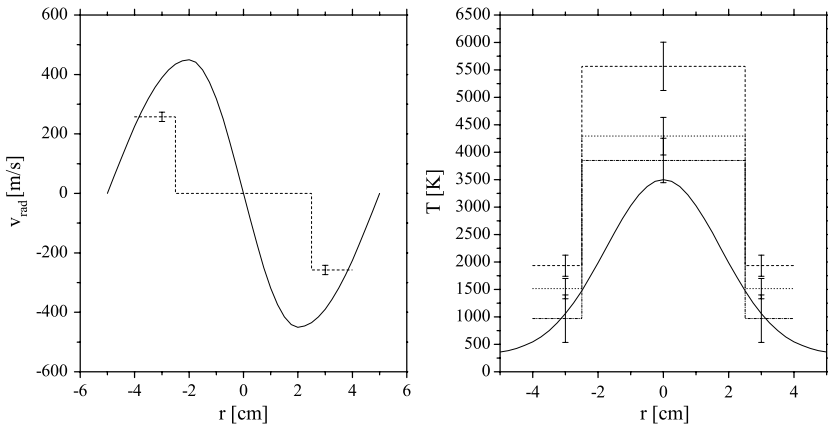

Figure 11. Comparison between v_r (left) and T (right) distributions along the jet radius obtained with the two models from the data shown in figure 6. The solid lines are distributions obtained with the more realistic model (see figure 10). Other lines correspond to results of the two-region model for several y positions: $y = 0$ cm (dashed), $y = 1$ cm (dotted) and $y = 2$ (dashed-dotted).

discussed in preceding sections, introducing a Doppler shift for the emitters leads to an overestimation of the temperature. In the light of previous arguments, the two-region model appears too simple to correctly describe the physical processes at work in plasma expansions. Therefore, one needs a more elaborated model of radiation transport that takes into account the smooth radial velocity distribution and the fact that emission and absorption occurs within the same volume.

In figure 11, the outcomes of the two models in terms of T and v_r distributions along the jet radius are compared with

one another. The distributions are obtained from best fits to experimental 763.5 nm Ar lineshapes shown in figure 6 and 9. In figure 11, error bars for the two-region model are deduced from the fitting procedure taking into account the uncertainty on the FP apparatus function. As can be seen in figure 11, the so-called more realistic model allows us to obtain smooth profiles that are in good agreement with the LIF data [20,21]. In contrast, outcomes of the two-region model are more doubtful. The boundary between the core and the surroundings of the plasma jets was fixed to $y = 2.5$ cm according to [21]. The radial velocity is found to be null within the core and around 250 m s^{-1} in the jet vicinity. The real velocity distribution is obviously more complex. Moreover the velocity must go back to zero far from the jet axis. The case of the temperature is even worst, as can be seen in figure 11. First, the Ar atom temperature is overestimated. Second, the temperature depends upon the y position, i.e. upon the chosen FP lineshape, and the differences between them are of the order of 50% of the smallest value. This analysis indicates that the two-region model can qualitatively explain the asymmetric line profiles; however, it fails in giving correct n, T and v_r values.

8. Conclusions

Determination of the plasma parameters from the measurements by optical emission spectroscopy is sometimes very difficult. Nevertheless, the comparison of measured radiation with the results of the modeling of radiation transport processes in the source may lead to better understanding and interpretation of measured data. This comparison may not be able to give the exact values of the plasma parameters as the spectral line profile depends on too many parameters in a similar way, but it can help to eliminate incorrect assumptions. The skewness of the reabsorbed lines is an assurance of both a significant radial velocity and a high atomic density in the lower state of the studied transition.

This work shows also that in the case of a plasma jet with significant velocity and divergence, the radial velocity component may affect the plasma emission in a way similar to the thermal velocity—it can broaden the lineshape. It means that the measurements of the translational temperature in a plasma jet by using the Doppler broadening measurement method can result in significant overestimation of the plasma temperature, even if the Abel transformation of the measured line profile is performed correctly.

Acknowledgments

The authors appreciate the technical assistance given by P Dom and N Gouillon. This work was carried out with the support of the Région Centre.

References

[1] Gomes A, Aubreton A, Gonzalez J J and Vacquie S 2004 *J. Phys. D: Appl. Phys.* **37** 689
[2] Marchesse Y, Gervais Y and Foulon H 2003 *AIAA J.* **41** 470
[3] Buuron A J M, Otorbaev D K, van de Sanden M C M and Schram D C 1994 *Phys. Rev.* E **50** 1383
[4] Zwicker H 1968 Evaluation of plasma parameters in optically thick plasmas *Plasma Diagnostics* ed W Lochte-Holtgreven (Amsterdam: North-Holland)
[5] Meulenbroeks R F G, van der HeijdenP A A, van de Sanden M C M and Schram D C 1994 *J. Appl. Phys.* **75** 2775
[6] Condrea I, Haddad E, Gregory B C and Abel G 2000 *Phys. Plasmas* **7** 3641
[7] Fusmmann G, Meyer H and Pasch E 1996 *Contrib. Plasma Phys.* **36** 501
[8] Vorlaufer G, Laimer J and Stori H 2000 *Meas. Sci. Technol.* **6** 1179
[9] Yan L, Xiao Z, Zhkong Y, Dong J, Deng Z, Li B, Li L, Feng Z, Liu Y and Wang E 2002 *Nucl. Fusion* **42** 265
[10] Kabouzi Y, Calzada M D, Moisan M, Tran K C and Trassy C 2002 *J. Appl. Phys.* **91** 1008
[11] Staicu A, Stolk R L and Ter Meulen J J 2002 *J. Appl. Phys.* **91** 969
[12] Tomassini P and Giulietti A 2001 *Opt. Commun.* **199** 143
[13] Kreye W C, Hemsky J W and Andrews M L 1993 *J. Phys. D: Appl. Phys.* **26** 1836
[14] Gueron S and Deutsch M 1996 *J. Appl. Phys.* **79** 8879
[15] Joshi N K , Sahasrabudhe S N, Sreekumar K P and Venkatramani N 1997 *Meas. Sci. Technol.* **8** 1146
[16] Kim C, Kim H G, Kim U J, Soo K I and Suk H 2004 *Rev. Sci. Instrum.* **75** 2865
[17] Kamińska A and Dudeck M 1999 *J. Tech. Phys.* **40** 33
[18] Schram D C, Mazouffre S, Engeln R, van de Sanden M C M 2001 *Atomic and Molecular Beams* ed R Campargue (New York: Springer) p 209
[19] Graur I A, Lengrand J C and Elizarova T G 2000 *Proc. 22nd Int. Symp. on Shock Waves (London, 2000)* ed G J Ball *et al* (London: Imperial College) vol 2 p 1267
[20] Engeln R, Mazouffre S, Vankan P, Schram D C and Sadeghi N 2001 *Plasma Sources Sci. Technol.* **10** 595
[21] Mazouffre S, Pawelec E, Caubet-Hilloutou V and Lengrand J-C 2005 *Phys. Plasmas* **12** 012323
[22] Mazouffre S, Pagon D, Lasgorceix P and Touzeau M 2003 *Proc. 28th Int. Electric Propulsion Conf.* (Toulouse, France) paper 283
[23] Gawron D, Mazouffre S and Boniface C 2006 *Plasma Sources Sci. Technol.* **15** 757
[24] Lochte-Holtgreven W 1968 Evaluation of plasma parameters *Plasma Diagnostics* ed W Lochte-Holtgreven (Amsterdam: North-Holland)
[25] Shayler P J and Fang M T C 1978 *J. Phys. D: Appl. Phys.* **11** 1743
[26] Perez J D and Payne G L 1980 *Phys. Rev.* A **21** 968
[27] Camargue R (ed) 2001 *Atomic and Molecular Beams* (New York: Springer)
[28] Mazouffre S 2001 Transport phenomena in plasma expansions containing hydrogen *PhD Thesis* Eindhoven University of Technology